

© 2019. This manuscript version is made available under the CC-BY-NC-ND 4.0 license <http://creativecommons.org/licenses/by-nc-nd/4.0/>

DOI: <https://doi.org/10.1016/j.tsf.2018.12.028>

A morphological and electronic study of ultrathin rear passivated Cu(In,Ga)Se₂ solar cells

S. Bose^{1,2#}, J.M.V. Cunha^{1,4}, J. Borme¹, W.C. Chen², N.S. Nilsson², J.P. Teixeira^{3,4}, J. Gaspar¹, J.P. Leitão^{3,4}, M. Edoff², P.A. Fernandes^{1,3,5}, P.M.P. Salomé^{1,4}

¹INL – International Iberian Nanotechnology Laboratory, Avenida Mestre José Veiga, 4715-330 Braga, Portugal

²Ångström Laboratory, Solid State Electronics, Ångström Solar Center, Uppsala University, SE-751 21 Uppsala, Sweden

³IN, Universidade de Aveiro, Campus Universitário de Santiago, 3810-193 Aveiro, Portugal

⁴Departamento de Física, Universidade de Aveiro, Campus Universitário de Santiago, 3810-193 Aveiro, Portugal

⁵Departamento de Física, Instituto Superior de Engenharia do Porto, Instituto Politécnico do Porto, Rua Dr. António Bernardino de Almeida 431, 4200-072 Porto, Portugal

#corresponding author: S. Bose, sourav.bose@inl.int

Abstract:

The effects of introducing a passivation layer at the rear of ultrathin Copper Indium Gallium di-Selenide Cu(In,Ga)Se₂ (CIGS) solar cells is studied. Point contact structures have been created on 25 nm Al₂O₃ layer using e-beam lithography. Reference solar cells with ultrathin CIGS layers provide devices with average values of light to power conversion efficiency of 8.1 % while for passivated cells values reached 9.5 %. Electronic properties of passivated cells have been studied before, but the influence of growing the CIGS on Al₂O₃ with point contacts was still unknown from a structural and morphological point of view. Scanning Electron Microscopy, X-ray Diffraction and Raman spectroscopy measurements were performed. These measurements revealed no significant morphological or structural differences in the CIGS layer for the passivated samples compared with reference samples. These results are in agreement with the similar values of carrier density ($\sim 8 \times 10^{16} \text{ cm}^{-3}$) and depletion region ($\sim 160 \text{ nm}$) extracted using electrical measurements. A detailed comparison between both sample types in terms of current-voltage, external quantum efficiency and photoluminescence measurements show very different optoelectronic behaviour which is indicative of a successful passivation. SCAPS simulations are done to explain the observed results in view of passivation of the rear interface.

Keywords

Passivation; Copper Indium Gallium di-Selenide; Solar cells; Ultrathin; Absorber; Thin film

1. Introduction

Thin film solar cells based on CIGS absorber layers have recently recorded a light to power conversion efficiency of 22.9% [1]. CIGS has thereby been increasing its great potential to be used as a promising absorber material for thin film solar cells. CIGS is a direct band-gap material having light absorption properties far larger than indirect bandgap materials such as Si. Hence, Si absorbers need to be sufficiently thick ($\sim 300 \mu\text{m}$) to absorb incoming photons. To reduce this thickness value, for economic reasons, advanced Si solar cell designs include a combination of an adequate rear surface passivation with micron-sized local point contacts and a rear reflector [2]. Application of this technology improves significantly the rear surface passivation and rear internal reflection, while enabling the use of thinner wafers from more than $300 \mu\text{m}$ to less than $200 \mu\text{m}$ [3]. For p-type Si solar cells, aluminium oxide (Al₂O₃), silicon

oxide (SiO_2) and silicon nitride (SiN_x) are the typical passivation layers used [4,5]. Industrial Laser technology is implemented in Si solar cells for the creation of the micron-sized openings on passivation layers [6–8]. We note that these concepts are still very incipient in CIGS technology. Techniques like formation and subsequent removal of spherical nano-particles in chemical bath deposition of CdS [3,9] and e-beam lithography [10–12] have been implemented in CIGS solar cells for the creation of nano-contact openings on rear passivation layers. Generally, high efficiency CIGS solar cells have absorber thickness ranging from 1.5 μm to 3 μm , and there are significant materials savings that can be achieved if this value is reduced to values lower than 500 nm. However, lowering of the absorber thickness causes degradation of solar cell performance and this has been systematically and experimentally studied by different groups since it is a topic of industrial and scientific relevance [3,9–22]. There are two main problems that occur when the absorber thickness is greatly reduced: (i) increase in the rear interface recombination and (ii) optical absorption losses. To compensate for the electrical degrading effects, local nano-sized point contacts are generated on the rear surface passivation layer [3,9–12,16,18,21,23,24]. In this way, rear contact recombination on the Mo-CIGS interface is significantly reduced due to sufficient coverage of the interface with the passivation layer, while the nano-contacts allow for charge carrier flow. Assuming short minority carrier lifetimes and thus short diffusion lengths, L_n -between 0.75 μm and 1.5 μm [3,9,25,26], for thin film CIGS solar cells the diameter of the contact openings are kept approximately to 200 nm while the pitch (the distance between two consecutive nano-contacts) is kept to 2 μm [3,9,11,12]. The passivation layer effectively lowers the rear interface recombination by lowering the number of interface defects (chemical passivation) and by the creation of a built-in electrical field (field-effect passivation) that repels minority carriers [27–29]. With regards to optical losses, several approaches are under study [18,21,23,24].

In this work, we provide detailed description of how the nanopatterning of the passivation layer is accomplished, but most importantly we focus on the effects of the incorporation of the passivation layer in the structural and morphological properties of the CIGS layer itself by X-ray diffraction (XRD) and Raman spectroscopy measurements. Additionally we also present the results of capacitance-voltage (C-V), external quantum efficiency (EQE) and current-voltage (J-V) measurements. Along with the experimental results, the rear passivation effects are simulated by SCAPS with a special emphasis on the influence of the effects of the rear interface recombination velocity in the cell performance.

2. Experimental Details

The solar cell device structure with rear surface passivated Al_2O_3 layer and ultrathin CIGS absorber (500 nm) is built up in the following way: SLG/Mo/ Al_2O_3 /CIGS/CdS/i:ZnO/ZnO:Al with Ni/Al/Ni front contacts. With the exception of the passivation layers and of the CIGS, all of the layers were produced according to the Ångström Base line and more information can be found in [3,9–12,21]. In addition, for the passivated cells a precursor Sodium fluoride (NaF) layer was evaporated just before the CIGS deposition. The NaF layer is not an addition to the final device structure as it used up in the CIGS during its deposition. The use and benefits of NaF is explained in the section 3.2 and also in the references [10–12,30–33]. The deposition sequence of different layers (upto the CIGS absorber) for both reference and passivated samples is illustrated in Fig. 1 (a & b).

An Al₂O₃ layer of 25 nm is sputtered using TIMARIS Flexible Target Module RF Sputter tool. The nano-sized point contacts on the Al₂O₃ layer is done with the use of e-beam lithography. Prior to the lithography process, 430 nm thick Polymethyl Methacrylate (PMMA) resist is spin-coated on the substrates (SLG-Mo-Al₂O₃) using spin coating. The substrates with resist are then exposed at 100 kV in a Vistec EBPG 5200 e-beam lithography system. A square array of dots with reproducible shapes (of equivalent diameters approx. 200 nm) and pitch size of 2 μm is produced in approximately 12 hours. The exposed resist is then developed using pure methylisobutylketone (MIBK) developer for 40 seconds in the e-beam track at room temperature. Anisotropic reactive ion etching (SPTS ICP) is done post development for the opening of the exposed dots on the Al₂O₃ layer. The PMMA is removed by dipping the sample in Acetone and treated in ultrasound for 15 minutes. Finally, the sample is cleaned in deionized (DI) water and subsequently dried under a N₂ blower.

During the CIGS absorber growth, the substrate temperature reaches up to 540 °C and have the compositional values of $[Cu]/([Ga] + [In])$ (CGI) = 0.85 ± 0.02 using an uniform through-depth $[Ga]/([Ga] + [In])$ (GGI) = 0.28 ± 0.01 ratio. The average CIGS thickness was 0.53 ± 0.03 μm as confirmed by X-ray fluorescence measurements and stylus profilometry, respectively. These ungraded (flat evaporation rate) CIGS absorbers are advantageous as they have high reproducibility and thereby assist the investigation of the rear surface passivation qualities. Each substrate has 12 cells and after scribing, each solar cell has an area of 0.5 cm². The presented solar cell results will be average of these 12 cells.

For the structural analysis of the CIGS in reference and rear passivated samples, x-ray diffraction (XRD) analysis have been done in Bragg-Brentano θ - 2θ configuration with a PanAnalytical X-Pert PRO MRD system with a CuK line of 1.5406 Å. For the analysis of surface modification of CIGS on the reference and passivated samples Raman spectroscopy was performed. A Confocal Raman Microscope 300 R (WiTec) with green laser excitation wavelength of 532 nm, 1 mW of laser power and a Zeiss objective of 100x in the backscattering configuration was used. Light J-V at AM1.5 and EQE measurements were performed in home-built systems. Scanning electron microscopy (SEM) images were taken in high resolution by a FEI Nova Nano 650 system using acceleration voltages of 3 kV and 5 kV. Capacitance-voltage (C-V) measurements were done in dark in Agilent E4980A LCR system with bias voltage ranging from -0.5 V to 0.5 V at 10 kHz bias frequency and amplitude of input signal, $V_{RMS} = 20$ mV. Photoluminescence measurements were performed in a Bruker Vertex 80 V spectrometer, equipped with an InGaAs detector. The excitation was done at the wavelength of 457.9 nm (spot diameter of ≈ 1 mm), with a laser power measured at the front of the cryostat window. Simulations of the solar cell were done using SCAPS 3.3 [3,11,34–38] to better understand the dissimilarities between reference and passivated solar cells with ultrathin CIGS absorbers.

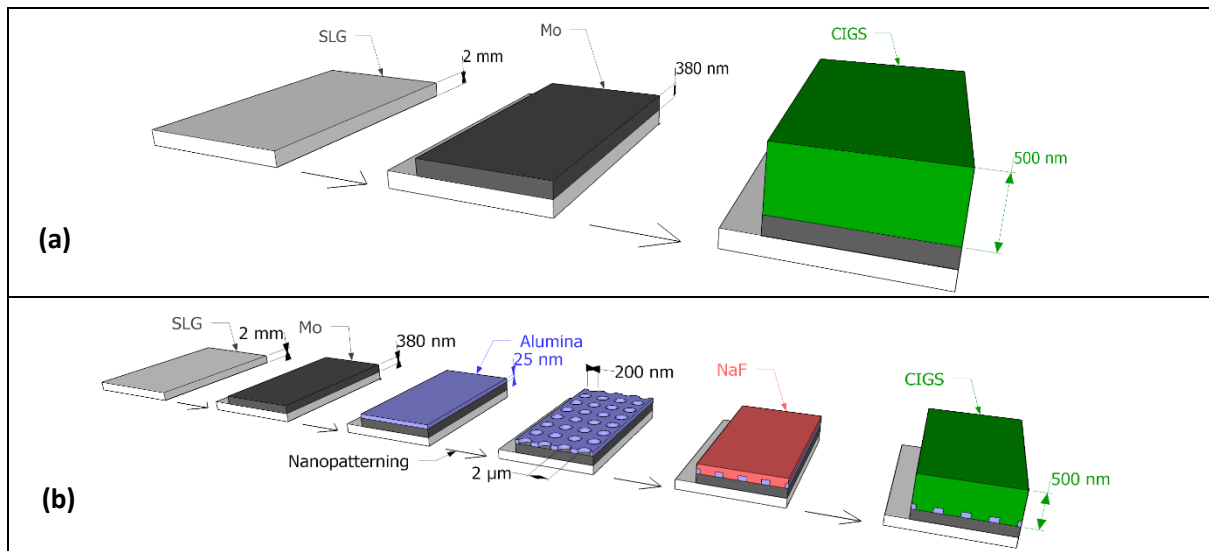


Fig. 1. Sequence of deposition steps (upto CIGS deposition) for (a) Reference and (b) Passivated Cells

3. Results and Discussion

3.1. Al_2O_3 passivation Layer with Nano-contacts created by e-beam

The application of e-beam lithography process generated the elliptically shaped nano-sized dots (point contacts) on the Al_2O_3 (25 nm) passivation layer. The top view of the well-ordered pattern of the nano point contacts are shown in Fig. 2a. The pitch and the nano-contact dimensions are shown in Fig. 2b. The images were taken post etch and photoresist stripping. The shape of the dot follows the symmetry of the e- beam during the exposure. The imperfection of the electron optics, in particular the astigmatism, leads to a beam elongated in a privileged direction. As a consequence, the imprinted dots are elliptic. The equivalent diameter is used as an estimation of the size of the dots, being obtained from the quadratic mean of the long axis and the short axis of the ellipses. The measurements were first taken from SEM images of a calibration sample after development with MIBK. The e-beam process could produce openings with a much better circular aspect at the expense of exposure time. As each 5x5 cm sample already takes approximately 12 hours, the use of the non-perfect circles is a compromise between exposure time and shape of the contact dot. Also visible in the picture of Fig. 1b is the normal morphology of Mo films, even with the Al_2O_3 layer deposited on top. Such fact means that the 25 nm Al_2O_3 are deposited in a conformal way minimizing micro/nano shunts.

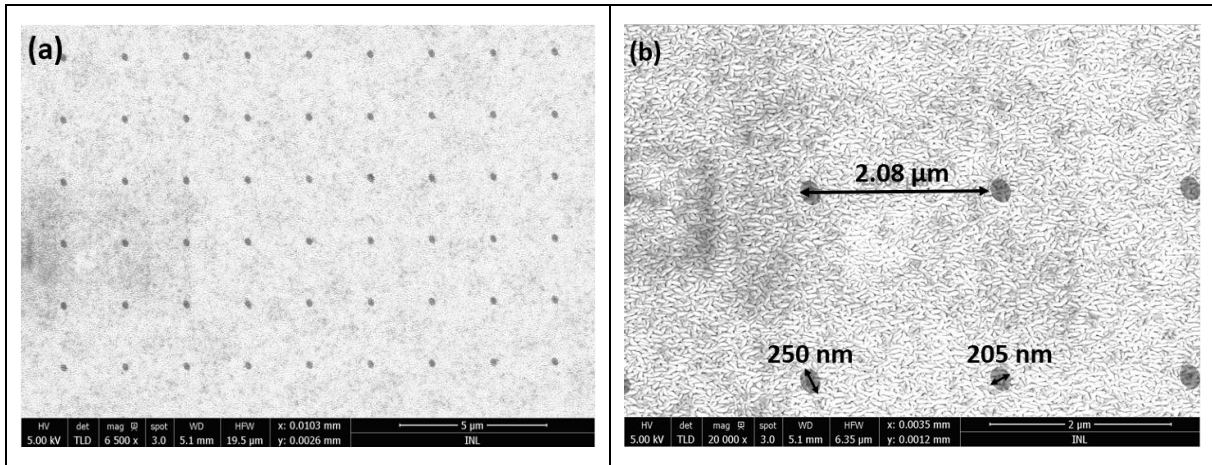


Fig. 2. SEM images of nano-contacts on the Al_2O_3 rear passivation layer: ; (a) shows the well-ordered pattern of the nano-contacts; (b) shows the pitch, the consecutive distance between two nano-contacts and the approximate longer and shorter dimensions of the elliptic nano-contacts are shown

In Fig. 3 (a & b) the top view of CIGS grains is shown for the reference and the passivated samples. (c & d) shows the cross-sectional views of the reference and passivated solar cells. Fig. 3d clearly displays the 25 nm thick Al_2O_3 rear passivated layer. Also, it is visible that the etching of the Al_2O_3 layer does not affect the back contact Mo layer. A careful SEM image analysis of the images reveals that the CIGS absorber does not undergo any significant morphological changes due to the effect of the Al_2O_3 passivation layer and the quality remains the same in both types of samples even after the complete fabrication of solar cells. The small grain size is typical for this type of flat profile samples that have not undergone a Cu-rich growth stage.

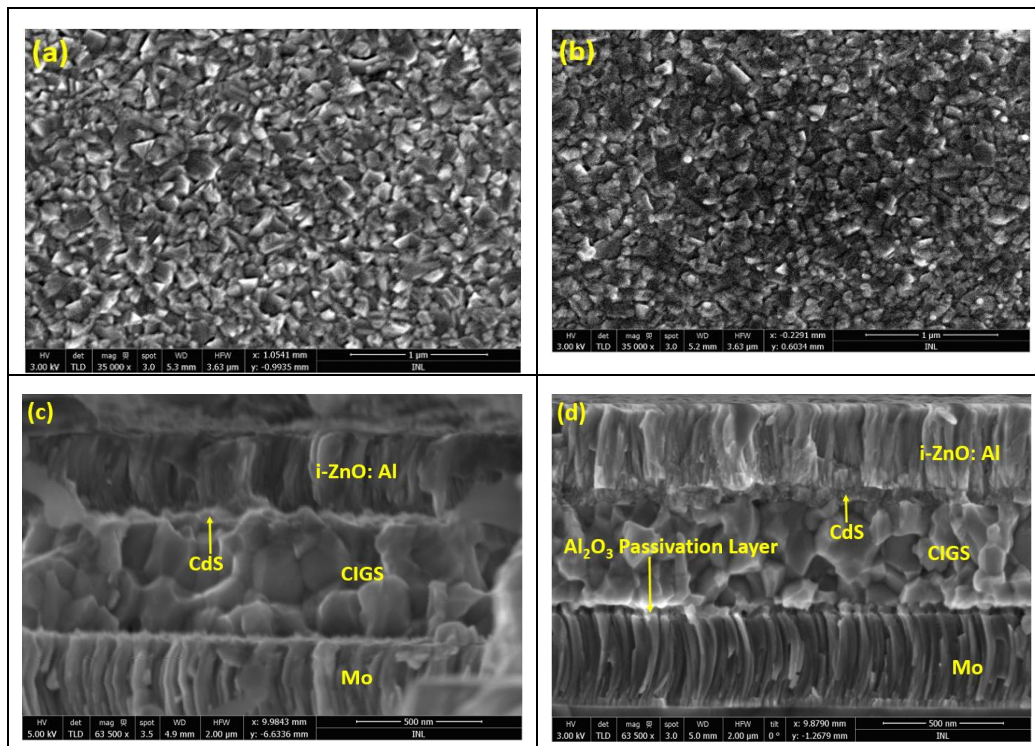


Fig. 3. Scanning electron microscopy images taken in different magnifications. (a) shows the CIGS grown on top of Mo only while (b) shows the CIGS grown on top of nano-patterned Al_2O_3 . In (c) & (d) magnified views of the

cross-section of the reference and rear passivated solar cells are shown. The presence of Al₂O₃ with the well-controlled pattern of nano-contacts does not affect the CIGS quality.

X-ray diffraction analysis followed the SEM analysis to better understand the structural changes (if any) for the CIGS on reference and passivated samples. The used Bragg-Brentano configuration is mostly a bulk measurement technique. In Fig. 4 (a & b) the XRD diffractograms are presented for the reference and passivated samples. It is seen in both diffractograms that the main CIGS XRD peak is present at 26.7° corresponding to the crystalline family planes (112). Other peaks are found for the crystalline planes (204) at 44.3° and (312/116) at 52.2° [39,40]. Prominent peaks are also found for Mo at 40.5° and for ZnO at 34.3° corresponding to the crystalline planes (110) and (111) respectively. It is noted for both the sample types that CdS peaks do not appear in the XRD diffractograms, as expected, as the layer is too thin to be probed by this analysis and it might even be in an amorphous state [41]. Also due to its very low thickness, the Al₂O₃ layer in the passivated sample does not result in any diffraction peaks. Overall analysis reveals that there are no significant changes in the CIGS due to the presence of the Al₂O₃ rear passivation layer.

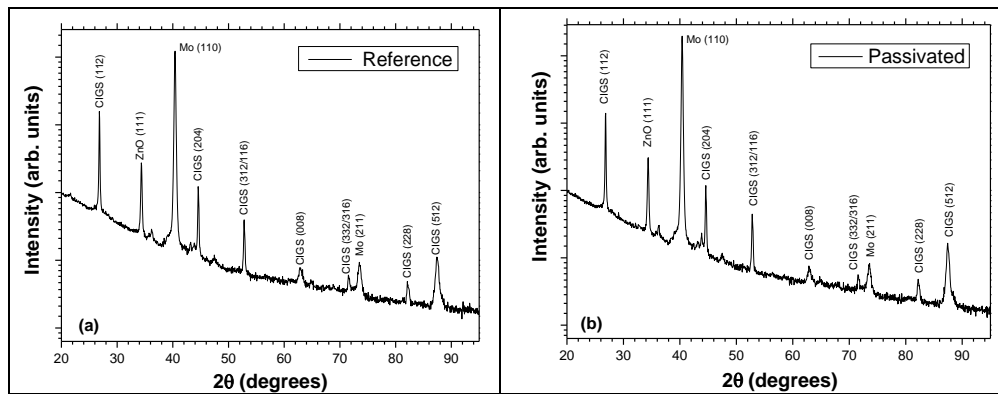


Fig. 4. (a) and (b) shows the XRD diffractograms of reference and passivated solar cells, respectively. The relative intensity peaks of CIGS related peaks for both the reference and the passivated solar cells remains unchanged.

TABLE I

RATIO OF XRD INTENSITIES FOR BOTH REFERENCE AND PASSIVATED SAMPLES AND FOR A POWDER SAMPLE

Sample Description	Intensity Ratio		
	$\frac{I_{112}}{I_{204}}$	$\frac{I_{112}}{I_{312}}$	$\frac{I_{204}}{I_{312}}$
Powder (Database)	1.75	3.43	1.96
Reference (Unpassivated)	3.03	4.94	1.63
Al ₂ O ₃ Rear Passivated	2.92	4.46	1.52

The intensity ratio values estimated for the Al₂O₃ rear passivated samples shows similar values to the ones for the reference samples (see TABLE I), indicating that Al₂O₃ has not changed the structural properties of the CIGS layer. Both ratios involving I_{112} show higher values for our CIGS films than for the powders, the powder diffraction data are for samples with infinite thickness. For our thin samples, the 112 peak, due to its glancing angle will have

a larger diffracted volume than the (204) and (312) peaks. So from the XRD point of view we can state that the CIGS in reference and passivated samples are similar.

To understand further if the deposition of the Al_2O_3 rear passivation layer causes any surface modifications to the CIGS or not, Raman spectroscopy was performed on the reference and the passivated samples. The solar cells were HCl etched, so that the layers above the CIGS layer are removed and the CIGS layer is exposed. Previous literature studies have shown that the HCl etch does not affect the CIGS layer [29,42]. So the Raman spectroscopy will provide information only about the structural changes to the CIGS layer down to a depth of 100 nm, which is very useful for ultra-thin devices with 500 nm absorber layer [43]. Representative curves for the Raman spectroscopy analysis are shown in the Fig. 5. Both samples reveal the CIGS A_1 mode peak located at 175.1 cm^{-1} [29,44–46]. This figure also shows the peaks fitting which allows to extract the spectra parameters. For the most prominent peak, A_1 mode, the fitting results show similar results with FWHM close to 6 cm^{-1} for both reference and passivated samples. Hence, we can say from the Raman analysis results that the CIGS on the Al_2O_3 passivated sample does not undergo any significant surface structural modifications in the probed region when compared with the reference sample.

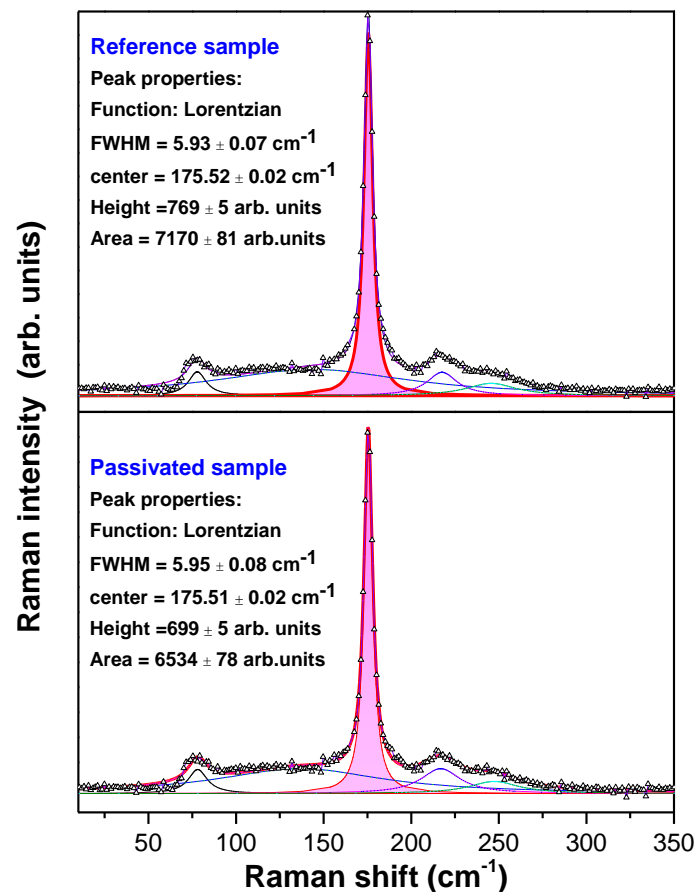


Fig. 5. Representative Raman spectra for reference and passivated samples along with fitting results.

3.2. Implementation of Al_2O_3 Passivation Layer into Ultrathin $\text{Cu}(\text{In,Ga})\text{Se}_2$ Solar Cells

The J-V analysis is summarized in Table II and representative J-V and EQE curves are shown in Fig. 6. An analysis of the implementation of the Al₂O₃ rear passivation layer with the nano-contacts into ultrathin CIGS solar cells reveals an increase in open circuit voltage (V_{oc}) and short circuit current density (J_{sc}) compared with the reference device. The improvements in the V_{oc} and J_{sc} could be due to the modifications in the rear surface passivation and likely also due to an increase in internal reflection. It is also noticed that there is a decrease in the fill factor (FF) for the rear passivated cells (64.7 %) compared with the reference value of 66.5 %. Nevertheless, the values of efficiency are higher for the rear passivated cells due to the combined improvements in V_{oc} and J_{sc}. Both solar cells have a CIGS absorber layer thickness of 500 nm. Comparison of the J-V and EQE for the reference and passivated cells is shown in Fig. 6 (a & b). The comparison shows that: (1) there is an increase in V_{oc} (+29 mV) due to the significant improvement in the rear passivation and (2) an increase in J_{sc} (+2.3 mA/cm²) due to the improvement of the rear internal reflection and/or passivation. This can also be seen in Fig. 6b, where we clearly see an increase in EQE for all wavelengths above 450 nm. The dark J-V plots for the reference and passivated shows no shunting while the light J-V plots shows shunting. So, the shunting effect is entirely light dependent. There is a cross-over effect on both reference and passivated samples, hence, this is not an effect of the introduction of the passivation layer. The cross-over effect on J-V curves is a continuous object of study in the literature and it is not yet fully understood. One possible explanation is that in the dark a large concentration of acceptors near the CIGS-CdS junction act as barrier. When illuminated these acceptors are fulfilled by the photogenerated carriers and the barrier is mitigated [47,48]. The cross-over is present for both reference and passivated samples, thus, the space charge region might be the same for both and it is in agreement with our results. A low fill factor (-4 % (abs.)), is noted for the passivated sample which could be due to the fact that ultra-thin devices have several recombination patterns. This should be further investigated. Similar changes in fill factor for passivated samples can be found in [17] and for a detailed electronic analysis [49] can be looked upon. Also, from the plot of Fig. 6c we see a higher difference of EQE between passivated and reference samples. This fact suggests the improved J_{sc} obtained for the passivated solar cells. The difference of EQE in the infrared region becomes lower which suggests that the poor response in the infrared region for both sample types is most probably due the rear collection issues and also due to the fact that ultra-thin CIGS absorbers suffers from incomplete photon absorption[12,13,18,19,50–52].

TABLE II

J-V CHARACTERIZATION RESULTS FOR REFERENCE AND Al₂O₃ REAR PASSIVATED CELLS WITH NANO-SIZED POINT CONTACTS

Sample Description	No. of Cells Analysed	V _{oc} (mV)	J _{sc} (mA/cm ²)	FF (%)	Efficiency (%)
Reference	12	573 ± 6	21.3 ± 1.0	66.5 ± 4.0	8.1 ± 0.5
Best Reference Cell	1	582	22.2	69.3	8.9
Al ₂ O ₃ Rear Passivated	12	609 ± 7	24.2 ± 0.9	64.7 ± 1.9	9.5 ± 0.2
Best Al ₂ O ₃ Rear Passivated Cell	1	611	24.5	65.3	9.8

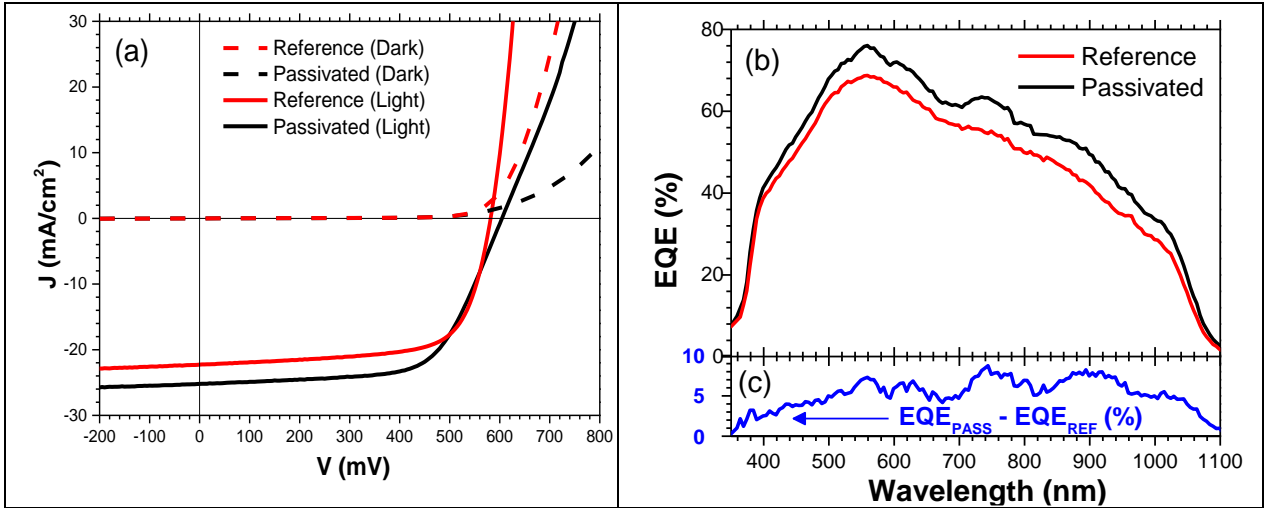


Fig. 6. (a) J-V and (b) external quantum efficiency (EQE) plots for reference and Al₂O₃ rear passivated CIGS solar cells. (c) Absolute difference of EQE (in %) between passivated and reference solar cells. CIGS absorber layer thickness for both types of cells is approximately 500 nm.

C-V measurements were done for the reference and Al₂O₃ rear passivated solar cells to obtain the width of the depletion region, ω (nm) at the CIGS-CdS interface and as well the net acceptors concentration, N_{CV} (cm⁻³) in the depletion region. These values are important to understand if the assumption that the CIGS doping and that the CIGS/CdS interface is different between both samples or not. ω and N_{CV} are extracted at 0 V without the effect of any external bias as commonly done [27,29,53,54], the resulting values are presented in Table III and representative curves are shown in Fig. 7. By analysing the results we see no significant changes in the electrical properties for the reference and passivated solar cells. The probed properties by this technique are strongly affected by the CIGS doping levels and by the CIGS/CdS interface. With regards to the CdS interface, as both samples were manufactured with the same conditions, a modification to the rear contact is very unlikely to be expected. However, due to the diffusion-blocking properties of the Al₂O₃ layer, a difference in sodium (Na) concentration in both samples might occur. Nonetheless, as the results from the C-V measurements are very similar, we can say that the Na concentration in the CIGS layer, that ultimately drives the doping levels, should be very similar in both samples. This is of particular importance as in the reference cell, Na is introduced via in-diffusion from the glass substrate, whereas for the passivated cell, a Sodium fluoride (NaF) precursor layer is used. Previous studies have shown that the CIGS has a threshold value of Na incorporation for what its properties are stable [30–33], which seems to be the point at what both samples are present. Hence, we can pinpoint even more that the modification in the J-V behaviour of both samples are very likely due to modifications of the rear passivation.

Fig. 8 shows the photoluminescence (PL) behaviour of both samples at 6 K with a laser excitation intensity of ~ 3 mW. For quantitative results, the PL analysis would need to be made with several dependencies like excitation power, temperature and wavelength. However, in this work we are using PL only to compare the samples qualitatively. We note that the luminescence in both samples have the same asymmetrical shape, common to highly doped semiconductor materials and also the passivated sample has a blue shift in its emission compared with the reference sample. These two facts are indications that the major recombination mechanism that dominates this emission is the same but that some

passivation of optically active defects occurred in the passivated sample that allowed a blue-shift of the emission [55–57]. These results are in very good agreement with the already presented ones showing that the CIGS properties are likely the same and that the rear interface recombination is being suppressed allowing for a blue shift of the emission translated in device terms into a higher V_{oc} value.

TABLE III

AVERAGE AND STANDARD DEVIATION VALUES OF ω AND M EXTRACTED BY C-V MEASUREMENTS FOR THE REFERENCE AND FOR THE Al_2O_3 REAR PASSIVATED CELLS

Sample Description	No. of Cells Analysed	ω (nm)	N_{cv} (cm^{-3})
Reference	12	165 ± 5	$(8.42 \pm 3.51)^{16}$
Al_2O_3 Rear Passivated	12	168 ± 8	$(6.53 \pm 2.19)^{16}$

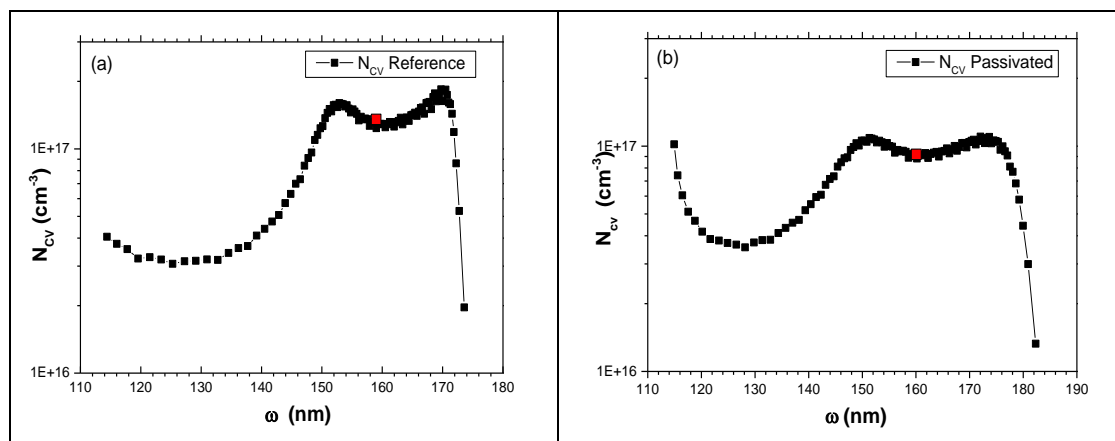


Fig. 7. Variation of the charge carrier concentration along the width of the depletion region for the (a) reference and (b) passivated solar cells. The red spots in the graphs shows the values for ω and N extracted at 0 V bias voltage.

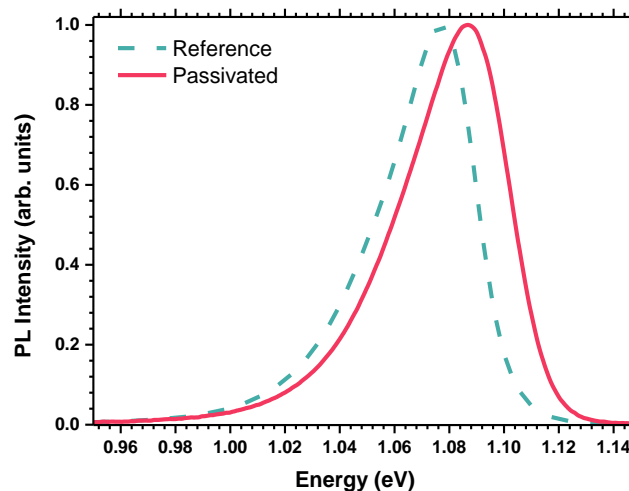


Fig. 8. Photoluminescence measured at 6 K under an excitation power of ~ 3 mW for the reference and Al_2O_3 rear passivated samples.

3.3. Modelling of Ultrathin $Cu(In,Ga)Se_2$ Solar Cells with Effects of Nano-patterned Al_2O_3 Rear Passivation Layer

SCAPS simulations [37,38] based on the model presented in the literatures [3,11,35,36] allow us to evaluate the degrading effects of lowering the thickness of the CIGS absorbers. The solar cell parameter results for CIGS solar cell with standard absorber thickness (1.5 μm) and with ultrathin CIGS (500 nm) are compared and shown in Table IV. The surface recombination velocity (S_b) is simulated in SCAPS for CIGS solar cells with 500 nm absorber thickness. As discussed above, the deposition of an Al_2O_3 rear passivation layer can significantly reduce S_b . We assumed as reference a value of 10^7 cm/s for the rear interface recombination velocity (S_b) [3,11,35]. The simulation results indicate that the approach of Al_2O_3 rear passivation layer for 500 nm CIGS solar cells has the potential to considerably increase the V_{oc} and thereby the efficiency. In a first instance, the main effect of changing the recombination velocity is to increase the V_{oc} , however after a significant decrease of S_b , J_{sc} starts to increase as well. The best solar cell (with NaF pre-treatment) with the nano-patterned Al_2O_3 rear passivation has V_{oc} 611 mV, J_{sc} 24.5 mA/cm², FF 65.3 % and efficiency of 9.8%. Without passivation, the V_{oc} comes down to 582 mV, J_{sc} to 22.2 mA/cm² and the efficiency to 8.9%. These experimental values provide for a difference in V_{oc} of 29 mV and of J_{sc} 2.3 mA/cm² after applying the passivation of the rear. With SCAPS simulations, we see that the V_{oc} can increase in this order of magnitude if S_b is expected to lower from 10^7 to values around 10^2 - 10^4 cm/s. In the simulations we have obtained very similar values for the figures of merit in comparison to the experimentally obtained results. Only the fill factor showed higher values and also thereby the efficiency since we are very far from the actual experimental conditions. This difference between the experimental and simulated values are expected, due to the fact that the model used in the simulation does not include all the loss mechanisms which are present in the real device. Nonetheless, it is possible to identify that there is still margin to progress with the quality of the passivation since a higher increase of the V_{oc} and of the J_{sc} is theoretically possible.

TABLE IV

SOLAR CELL PARAMETER RESULTS FROM SCAPS SHOWING THE EFFECT OF LOWERING THE THICKNESS OF THE ABSORBER AND OF CHANGING THE RECOMBINATION VELOCITY (S_b)

CIGS Absorber Thickness (nm)	S_b (cm/s)	V_{oc} (mV)	J_{sc} (mA/cm²)	FF (%)	Efficiency (%)
1500	10^7	658	30.23	79.9	15.94
500	10^7	536	24.20	72.58	9.43
500	10^6	544	24.29	72.88	9.63
500	10^5	546	24.48	73.42	9.82
500	10^4	566	25.21	73.57	10.51
500	10^3	573	27.29	77.50	12.01
500	10^2	610	27.59	77.82	13.11

4. Conclusion and Outlook

From our careful analysis we summarize that the nano-patterned Al₂O₃ rear-surface passivation layer created by e-beam lithography technology can be implemented for performance enhancement of CIGS solar cells and that its introduction does not change the CIGS crystalline properties. Ultrathin CIGS absorber layers with the rear passivation show an improvement in all the solar cell parameters with respect to unpassivated reference cells and without undergoing any significant structural or morphological changes. Additionally, the cells with ultrathin CIGS absorbers have been modelled with SCAPS to understand the effects of rear passivation. SCAPS modelling results indicates a performance degradation with lowering the absorber thickness to 500 nm, but implementation of the rear passivation effects by reducing the charge carrier recombination velocity an improvement in performance is noticed. As no significant structural and morphological changes are noticed in the CIGS absorber, nano-patterns of different dimensions along with different thickness of the passivation layer can be tested in the future.

Acknowledgements

P.M.P. Salomé acknowledges the funding of Fundação para a Ciência e a Tecnologia (FCT) through the project IF/00133/2015. The European Union's Horizon 2020 research and innovation programme ARCIQS-M project (grant agreement no. 720887) is acknowledged. J. M. V. Cunha acknowledges the funding of Fundação para a Ciência e a Tecnologia (FCT) through the project PD/BD/142780/2018. J. P. Teixeira and J. P. Leitão acknowledge the funding of FCT through the project UID/CTM/50025/2013.

References

- [1] M.A. Green, Y. Hishikawa, E.D. Dunlop, D.H. Levi, J. Hohl-Ebinger, A.W.Y. Ho-Baillie, Solar cell efficiency tables (version 52), *Progress in Photovoltaics: Research and Applications*. 26 (2018) 427–436. doi:10.1002/pip.3040.
- [2] J. Zhao, A. Wang, M.A. Green, 24% efficient PERL structure silicon solar cells, in: *IEEE Conference on Photovoltaic Specialists*, 1990: pp. 333–335 vol.1. doi:10.1109/PVSC.1990.111642.
- [3] B. Vermang, V. Fjällström, J. Pettersson, P. Salomé, M. Edoff, Development of rear surface passivated Cu(In,Ga)Se₂ thin film solar cells with nano-sized local rear point contacts, *Solar Energy Materials and Solar Cells*. 117 (2013) 505–511. doi:10.1016/j.solmat.2013.07.025.
- [4] B. Vermang, H. Goverde, L. Tous, A. Lorenz, P. Choulat, J. Horzel, J. John, J. Poortmans, R. Mertens, Approach for Al₂O₃ rear surface passivation of industrial p-type Si PERC above 19%, *Progress in Photovoltaics: Research and Applications*. 20 (2012) 269–273. doi:10.1002/pip.2196.
- [5] T. Dullweber, S. Gatz, H. Hannebauer, T. Falcon, R. Hesse, J. Schmidt, R. Brendel, Towards 20% efficient large-area screen-printed rear-passivated silicon solar cells, *Progress in Photovoltaics: Research and Applications*. 20 (2012) 630–638. doi:10.1002/pip.1198.
- [6] M. Moors, K. Baert, T. Caremans, F. Duerinckx, A. Cacciato, J. Szlufcik, Industrial PERL-type solar cells exceeding 19% with screen-printed contacts and homogeneous emitter, *Solar Energy Materials and Solar Cells*. 106 (2012) 84–88. doi:10.1016/j.solmat.2012.05.006.
- [7] G. Agostinelli, J. Szlufcik, P. Choulat, G. Beaucarne, Local contact structures for

- industrial PERC-type solar cells, in: Proc. 20th Eur. Photovoltaic Sol. Energy Conf., 2005: pp. 942–945.
- [8] E. Schneiderlöchner, R. Preu, R. Lüdemann, S.W. Glunz, Laser-fired rear contacts for crystalline silicon solar cells, *Progress in Photovoltaics: Research and Applications*. 10 (2002) 29–34. doi:10.1002/pip.422.
- [9] B. Vermang, V. Fjallstrom, X. Gao, M. Edoff, Improved Rear Surface Passivation of Cu(In,Ga)Se₂ Solar Cells: A Combination of an Al₂O₃ Rear Surface Passivation Layer and Nanosized Local Rear Point Contacts, *IEEE Journal of Photovoltaics*. 4 (2014) 486–492. doi:10.1109/JPHOTOV.2013.2287769.
- [10] B. Vermang, J.T. Wätjen, V. Fjällström, F. Rostvall, M. Edoff, R. Kotipalli, F. Henry, D. Flandre, Employing Si solar cell technology to increase efficiency of ultra-thin Cu(In,Ga)Se₂ solar cells, *Progress in Photovoltaics: Research and Applications*. 22 (2014) 1023–1029. doi:10.1002/pip.2527.
- [11] B. Vermang, J.T. Watjen, C. Frisk, V. Fjallstrom, F. Rostvall, M. Edoff, P. Salome, J. Borme, N. Nicoara, S. Sadewasser, Introduction of Si PERC Rear Contacting Design to Boost Efficiency of Cu(In,Ga)Se₂ Solar Cells, *IEEE Journal of Photovoltaics*. 4 (2014) 1644–1649. doi:10.1109/JPHOTOV.2014.2350696.
- [12] P.M.P. Salomé, B. Vermang, R. Ribeiro-Andrade, J.P. Teixeira, J.M. V. Cunha, M.J. Mendes, S. Haque, J. Borme, H. Águas, E. Fortunato, R. Martins, J.C. González, J.P. Leitão, P.A. Fernandes, M. Edoff, S. Sadewasser, Passivation of Interfaces in Thin Film Solar Cells: Understanding the Effects of a Nanostructured Rear Point Contact Layer, *Advanced Materials Interfaces*. 5 (2018) 1701101. doi:10.1002/admi.201701101.
- [13] O. Lundberg, M. Bodegård, J. Malmström, L. Stolt, Influence of the Cu(In,Ga)Se₂ thickness and Ga grading on solar cell performance, *Progress in Photovoltaics: Research and Applications*. 11 (2003) 77–88. doi:10.1002/pip.462.
- [14] K. Ramanathan, R. Noufi, B. To, D. I. Young, R. Bhattacharya, M.A. Contreras, R.G. Dhere, G. Teeter, Processing and Properties of Sub-Micron CIGS Solar Cells, in: 2006 IEEE 4th World Conference on Photovoltaic Energy Conference, 2006: pp. 380–383. doi:10.1109/WCPEC.2006.279469.
- [15] E. Jarzembowski, M. Maiberg, F. Obereigner, K. Kaufmann, S. Krause, R. Scheer, Optical and electrical characterization of Cu(In,Ga)Se₂ thin film solar cells with varied absorber layer thickness, *Thin Solid Films*. 576 (2015) 75–80. doi:10.1016/j.tsf.2015.01.004.
- [16] D. Ledinek, P. Salome, C. Hagglund, U. Zimmermann, M. Edoff, Rear Contact Passivation for High Bandgap Cu(In, Ga)Se₂ Solar Cells With a Flat Ga profile, *IEEE Journal of Photovoltaics*. 8 (2018) 864–870. doi:10.1109/JPHOTOV.2018.2813259.
- [17] S. Bose, J.M. V. Cunha, S. Suresh, J. De Wild, T.S. Lopes, J.R.S. Barbosa, R. Silva, J. Borme, P.A. Fernandes, B. Vermang, P.M.P. Salomé, Optical Lithography Patterning of SiO₂ Layers for Interface Passivation of Thin Film Solar Cells, *Solar RRL*. (2018) 1800212. doi:10.1002/solr.201800212.
- [18] N. Naghavi, F. Mollica, J. Goffard, J. Posada, A. Duchatelet, M. Jubault, F. Donsanti, A. Cattoni, S. Collin, P.P. Grand, J.J. Greffet, D. Lincot, Ultrathin Cu(In,Ga)Se₂ based solar cells, *Thin Solid Films*. 633 (2017) 55–60. doi:10.1016/j.tsf.2016.11.029.
- [19] Z.J. Li-Kao, N. Naghavi, F. Erfurth, J.F. Guillemoles, I. Gérard, A. Etcheberry, J.L. Pelouard, S. Collin, G. Voorwinden, D. Lincot, Towards ultrathin copper indium gallium diselenide solar cells: proof of concept study by chemical etching and gold back contact engineering, *Progress in Photovoltaics: Research and Applications*. 20 (2012) 582–587. doi:10.1002/pip.2162.

- [20] J. Pettersson, T. Törndahl, C. Platzer-Björkman, A. Hultqvist, M. Edoff, The Influence of Absorber Thickness on Cu(In,Ga)Se₂ Solar Cells With Different Buffer Layers, *IEEE Journal of Photovoltaics*. 3 (2013) 1376–1382. doi:10.1109/JPHOTOV.2013.2276030.
- [21] B. Vermang, J.T. Wätjen, V. Fjällström, F. Rostvall, M. Edoff, R. Gunnarsson, I. Pilch, U. Helmersson, R. Kotipalli, F. Henry, D. Flandre, Highly reflective rear surface passivation design for ultra-thin Cu(In,Ga)Se₂ solar cells, *Thin Solid Films*. 582 (2015) 300–303. doi:10.1016/j.tsf.2014.10.050.
- [22] T. Negami, S. Nishiwaki, Y. Hashimoto, N. Kohara, T. Wada, Effect of absorber thickness on performance of Cu(In,Ga)Se₂ solar cells, in: *Proceedings of the 2nd WCPEC 1998, 1998*: pp. 1181–1184.
- [23] C. van Lare, G. Yin, A. Polman, M. Schmid, Light Coupling and Trapping in Ultrathin Cu(In,Ga)Se₂ Solar Cells Using Dielectric Scattering Patterns, *ACS Nano*. 9 (2015) 9603–9613. doi:10.1021/acsnano.5b04091.
- [24] G. Yin, P. Manley, M. Schmid, Light trapping in ultrathin CuIn_{1-x}Ga_x Se₂ solar cells by dielectric nanoparticles, *Solar Energy*. 163 (2018) 443–452. doi:10.1016/j.solener.2018.01.096.
- [25] G. Brown, V. Faifer, A. Pudov, S. Anikeev, E. Bykov, M. Contreras, J. Wu, Determination of the minority carrier diffusion length in compositionally graded Cu(In,Ga)Se₂ solar cells using electron beam induced current, *Applied Physics Letters*. 96 (2010) 22104. doi:10.1063/1.3291046.
- [26] R. Kniese, M. Powalla, U. Rau, Evaluation of electron beam induced current profiles of Cu(In,Ga)Se₂ solar cells with different Ga-contents, *Thin Solid Films*. 517 (2009) 2357–2359. doi:10.1016/j.tsf.2008.11.049.
- [27] R. Kotipalli, B. Vermang, J. Joel, R. Rajkumar, M. Edoff, D. Flandre, Investigating the electronic properties of Al₂O₃/Cu(In,Ga)Se₂ interface, *AIP Advances*. 5 (2015) 107101. doi:10.1063/1.4932512.
- [28] W.-W. Hsu, J.Y. Chen, T.-H. Cheng, S.C. Lu, W.-S. Ho, Y.-Y. Chen, Y.-J. Chien, C.W. Liu, Surface passivation of Cu(In,Ga)Se₂ using atomic layer deposited Al₂O₃, *Applied Physics Letters*. 100 (2012) 23508. doi:10.1063/1.3675849.
- [29] J.M. V. Cunha, P.A. Fernandes, A. Hultqvist, J.P. Teixeira, S. Bose, B. Vermang, S. Garud, D. Buldu, J. Gaspar, M. Edoff, J.P. Leitão, P.M.P. Salomé, Insulator Materials for Interface Passivation of Cu(In,Ga)Se₂ Thin Films, *IEEE Journal of Photovoltaics*. 8 (2018) 1313–1319. doi:10.1109/JPHOTOV.2018.2846674.
- [30] P.M.P. Salomé, A. Hultqvist, V. Fjällström, M. Edoff, B. Aitken, K. Vaidyanathan, K. Zhang, K. Fuller, C. Kosik Williams, Cu(In,Ga)Se₂ Solar Cells With Varying Na Content Prepared on Nominally Alkali-Free Glass Substrates, *IEEE Journal of Photovoltaics*. 3 (2013) 852–858. doi:10.1109/JPHOTOV.2013.2247655.
- [31] M. Bodeg Ård, K. Granath, L. Stolt, Growth of Cu(In,Ga)Se₂ thin films by coevaporation using alkaline precursors, *Thin Solid Films*. 361–362 (2000) 9–16. doi:10.1016/S0040-6090(99)00828-7.
- [32] P.M.P. Salomé, H. Rodriguez-Alvarez, S. Sadewasser, Incorporation of alkali metals in chalcogenide solar cells, *Solar Energy Materials and Solar Cells*. 143 (2015) 9–20. doi:10.1016/j.solmat.2015.06.011.
- [33] P.M.P. Salome, A. Hultqvist, V. Fjallstrom, M. Edoff, B.G. Aitken, K. Zhang, K. Fuller, C. Kosik Williams, Incorporation of Na in Cu(In,Ga)Se₂ Thin-Film Solar Cells: A Statistical Comparison Between Na From Soda-Lime Glass and From a Precursor Layer of NaF, *IEEE Journal of Photovoltaics*. 4 (2014) 1659–1664.

- doi:10.1109/JPHOTOV.2014.2357261.
- [34] R. Kotipalli, O. Poncelet, G. Li, Y. Zeng, L.A. Francis, B. Vermang, D. Flandre, Addressing the impact of rear surface passivation mechanisms on ultra-thin Cu(In,Ga)Se₂ solar cell performances using SCAPS 1-D model, *Solar Energy*. 157 (2017) 603–613. doi:10.1016/j.solener.2017.08.055.
- [35] N. Touafek, R. Mahamdi, Back Surface Recombination Effect on the Ultra-Thin CIGS Solar Cells by SCAPS, *International Journal of Renewable Energy Research*. 4 (2014) 958.
- [36] H. Heriche, Z. Rouabah, N. Bouarissa, New ultra thin CIGS structure solar cells using SCAPS simulation program, *International Journal of Hydrogen Energy*. 42 (2017) 9524–9532. doi:10.1016/j.ijhydene.2017.02.099.
- [37] M. Burgelman, P. Nollet, S. Degrove, Modelling polycrystalline semiconductor solar cells, *Thin Solid Films*. 361–362 (2000) 527–532. doi:10.1016/S0040-6090(99)00825-1.
- [38] J. Verschraegen, M. Burgelman, Numerical modeling of intra-band tunneling for heterojunction solar cells in scaps, *Thin Solid Films*. 515 (2007) 6276–6279. doi:10.1016/j.tsf.2006.12.049.
- [39] B. Li, Y. Xie, J. Huang, Y. Qian, Synthesis by a Solvothermal Route and Characterization of CuInSe₂ Nanowhiskers and Nanoparticles, *Advanced Materials*. 11 (1999) 1456–1459. doi:10.1002/(SICI)1521-4095(199912)11:17<1456::AID-ADMA1456>3.0.CO;2-3.
- [40] T.A. Reese, S.B. Schujman, R.J. Matyi, Structure evolution in CIGS deposition: An X-ray diffraction analysis with Rietveld whole-pattern refinement, in: 2014 IEEE 40th Photovoltaic Specialist Conference (PVSC), 2014: pp. 1691–1695. doi:10.1109/PVSC.2014.6925246.
- [41] F. Mollica, Optimization of ultra-thin Cu(In,Ga)Se₂ based solar cells with alternative back-contacts, PhD Thesis, Université Pierre et Marie Curie - Paris VI, 2016.
- [42] D. Liao, A. Rockett, Cd doping at the CuInSe₂/CdS heterojunction, *Journal of Applied Physics*. 93 (2003) 9380–9382. doi:10.1063/1.1570500.
- [43] P.D. Paulson, R.W. Birkmire, W.N. Shafarman, Optical characterization of CuIn_{1-x}Ga_xSe₂ alloy thin films by spectroscopic ellipsometry, *Journal of Applied Physics*. 94 (2003) 879–888. doi:10.1063/1.1581345.
- [44] J. Bi, L. Yao, J. Ao, S. Gao, G. Sun, Q. He, Z. Zhou, Y. Sun, Y. Zhang, Pulse electro-deposition of copper on molybdenum for Cu(In,Ga)Se₂ and Cu₂ZnSnSe₄ solar cell applications, *Journal of Power Sources*. 326 (2016) 211–219. doi:10.1016/j.jpowsour.2016.07.005.
- [45] J. Wang, J. Zhu, Y.X. He, The influence of different locations of sputter guns on the morphological and structural properties of Cu–In–Ga precursors and Cu(In,Ga)Se₂ thin films, *Applied Surface Science*. 288 (2014) 109–114. doi:10.1016/j.apsusc.2013.09.154.
- [46] R. Scheer, A. Pérez-Rodríguez, W.K. Metzger, Advanced diagnostic and control methods of processes and layers in CIGS solar cells and modules, *Progress in Photovoltaics: Research and Applications*. 18 (2010) 467–480. doi:10.1002/pip.966.
- [47] R. Scheer, H.-W. Schock, *Chalcogenide Photovoltaics*, Wiley-VCH Verlag GmbH & Co. KGaA, Weinheim, Germany, 2011. doi:10.1002/9783527633708.
- [48] A. Niemegeers, M. Burgelman, R. Herberholz, U. Rau, D. Hariskos, H.-W. Schock, Model for electronic transport in Cu(In,Ga)Se₂ solar cells, *Progress in Photovoltaics: Research and Applications*. 6 (1998) 407–421. doi:10.1002/(SICI)1099-159X(199811/12)6:6<407::AID-PIP230>3.0.CO;2-U.
- [49] R. Scheer, Towards an electronic model for CuIn_{1-x}Ga_xSe₂ solar cells, *Thin Solid Films*.

- 519 (2011) 7472–7475. doi:10.1016/j.tsf.2011.01.092.
- [50] Z. Jehl, F. Erfurth, N. Naghavi, L. Lombez, I. Gerard, M. Bouttemy, P. Tran-Van, A. Etcheberry, G. Voorwinden, B. Dimmler, W. Wischmann, M. Powalla, J.F. Guillemoles, D. Lincot, Thinning of CIGS solar cells: Part II: Cell characterizations, *Thin Solid Films*. 519 (2011) 7212–7215. doi:10.1016/j.tsf.2010.12.224.
- [51] N. Naghavi, Z. Jehl, F. Donsanti, J.-F. Guillemoles, I. Gérard, M. Bouttemy, A. Etcheberry, J.-L. Pelouard, S. Collin, C. Colin, N. Péré-Laperne, N. Dahan, J.-J. Greffet, B. Morel, Z. Djebbour, A. Darga, D. Mencaraglia, G. Voorwinden, B. Dimmler, M. Powalla, D. Lincot, Toward high efficiency ultra-thin CIGSe based solar cells using light management techniques, in: A. Freundlich, J.-F.F. Guillemoles (Eds.), *Proc. SPIE 8256*, 2012: p. 825617. doi:10.1117/12.909419.
- [52] B. Vermang, J.T. Wätjen, V. Fjällström, F. Rostvall, M. Edoff, R. Gunnarsson, I. Pilch, U. Helmersson, R. Kotipalli, F. Henry, D. Flandre, Highly reflective rear surface passivation design for ultra-thin Cu(In,Ga)Se₂ solar cells, *Thin Solid Films*. 582 (2015) 300–303. doi:10.1016/j.tsf.2014.10.050.
- [53] J. Hllibrand, R.D. Gold, Determination of the impurity distribution in junction diodes from capacitance-voltage measurements, in: *Semiconductor Devices: Pioneering Papers*, S.M.Sze, Ed., World Scientific, 1991: pp. 191–198. doi:10.1142/9789814503464_0019.
- [54] R. Kotipalli, Surface Passivation Effects of Aluminium Oxide on Ultra-Thin CIGS Solar Cells, PhD Thesis, Ecole Polytechnique De Louvain, 2016.
- [55] J.P. Teixeira, R.A. Sousa, M.G. Sousa, A.F. da Cunha, P.A. Fernandes, P.M.P. Salomé, J.P. Leitão, Radiative transitions in highly doped and compensated chalcopyrites and kesterites: The case of Cu₂ZnSnS₄, *Physical Review B*. 90 (2014) 235202. doi:10.1103/PhysRevB.90.235202.
- [56] P.M.P. Salomé, J.P. Teixeira, J. Keller, T. Törndahl, S. Sadewasser, J.P. Leitão, Influence of CdS and ZnSnO Buffer Layers on the Photoluminescence of Cu(In,Ga)Se₂ Thin Films, *IEEE Journal of Photovoltaics*. 7 (2017) 670–675. doi:10.1109/JPHOTOV.2016.2639347.
- [57] N. Ben Sedrine, R. Ribeiro-Andrade, A. Gustafsson, M.R. Soares, J. Bourgard, J.P. Teixeira, P.M.P. Salomé, M.R. Correia, M.V.B. Moreira, A.G. De Oliveira, J.C. González, J.P. Leitão, Fluctuating potentials in GaAs:Si nanowires: critical reduction of the influence of polytypism on the electronic structure, *Nanoscale*. 10 (2018) 3697–3708. doi:10.1039/C7NR08395E.